IJMMM International Journal of Minerals, Metallurgy and Materials 矿物冶金与材料学报（英文版）

Mica-stabilized polyethylene glycol composite phase change materials for thermal energy storage

Dongyao Zhang, Chuanchang Li, Niangzhi Lin, Baoshan Xie, and Jian Chen

Cite this article as:
Dongyao Zhang, Chuanchang Li, Niangzhi Lin, Baoshan Xie, and Jian Chen, Mica-stabilized polyethylene glycol composite phase change materials for thermal energy storage, *Int. J. Miner. Metall. Mater.*, 29(2022), No. 1, pp. 168-176. https://doi.org/10.1007/s12613-021-2357-4

International Journal of Minerals, Metallurgy and Materials
Volume 29, Number 1, January 2022, Page 168
https://doi.org/10.1007/s12613-021-2357-4

Mica-stabilized polyethylene glycol composite phase change materials for thermal energy storage

Dongyao Zhang, Chuanchang Li✉, *Niangzhi Lin, Baoshan Xie, and Jian Chen*

School of Energy and Power Engineering, Changsha University of Science and Technology, Changsha 410114, China
(Received: 5 July 2021; revised: 28 August 2021; accepted: 23 September 2021)

Abstract: Mica was used as a supporting matrix for composite phase change materials (PCMs) in this work because of its distinctive morphology and structure. Composite PCMs were prepared using the vacuum impregnation method, in which mica served as the supporting material and polyethylene glycol (PEG) served as the PCM. Fourier transform infrared and X-ray diffraction analysis confirmed that the addition of PEG had no effect on the crystal structure of mica. Moreover, no chemical reaction occurred between PEG and mica during the vacuum impregnation process, and no new substance was formed. The maximum load of mica-stabilized PEG was 46.24%, the phase change temperature of M_{400}/PEG was 46.03°C, and the latent heat values of melting and cooling were 77.75 and 77.73 $J \cdot g^{-1}$, respectively. The thermal conductivity of M_{400}/PEG was 2.4 times that of pure PEG. The thermal infrared images indicated that the thermal response of M_{400}/PEG improved relative to that of pure PEG. The leakage test confirmed that mica could stabilize PEG and that M_{400}/PEG had great form-stabilized property. These results demonstrate that M_{400}/PEG has potential in the field of building energy conservation.

Keywords: mica; polyethylene glycol; phase change materials; thermal energy storage

1. Introduction

As a type of renewable energy with great potentiality, solar energy has become a major consideration in many countries all over the world [1–4]. However, in the conversion and use of solar energy, low conversion sufficiency and the contradiction between time supply and demand present serious issues [5]. Thermal energy storage (TES) technology can realize the storage of thermal energy, improve the efficiency of energy use, and address the imbalance between energy supply and demand [6–10]. As the core of TES, thermal storage materials have been widely used in many fields, such as building energy efficiency, concentrated solar power, solar thermal storage, and industrial waste heat recovery applications [11–13]. However, the high cost of preparing thermal storage materials limits the development of their applications in these fields. Therefore, the preparation and application of high-performance and low-cost thermal storage materials are of great significance.

Thermal storage materials that use latent heat to store energy have received unprecedented attention [14–16]. Phase change materials (PCMs) with high energy storage density and near-isothermal process are widely used in applications with diverse energy utilization, including photovoltaic thermal management [17], solar water heater systems [18], building energy efficiency [19], lithium-ion battery thermal management [20–21], wearable fabric [22–23], photon application field [24–25], high-temperature energy storage [26], and smart windows [27–28]. By adding PCMs to ordinary building materials to prepare phase change energy storage building materials with large heat storage capacity, indoor temperature fluctuations are reduced, and the thermal storage capacity of envelope structures is improved, thereby effectively reducing building energy consumption and achieving energy saving and emission reduction [29]. Organic PCMs with great TES performance, stable phase change temperature, good chemical stability, and low corrosion have attracted increasing attention [30–31]. However, PCMs still suffer from some defects, such as leakage during solid–liquid transformation [32–33], low thermal conductivity [34–35], and poor thermal stability [36], all of which hinder the practical applications of these materials. Several methods have been adopted to improve these defects, and they include the use of porous support materials to limit PCMs [37], mixing of high thermal conductivity materials, and the use of microencapsulated PCMs [38]. Impregnating PCMs into porous matrices to prepare shape-stabilized composite materials has become a research focus [39–40].

Mica is a type of flaky silicate mineral with complete laminar dissociation. Mica exhibits high insulation performance, great chemical stability, strong acidity, strong alkalinity, and good compression resistance. Hence, it has been widely used in buildings, fire control, papermaking, and rubber manufacturing. Few reports have detailed the application of mica in

✉ Corresponding author: Chuanchang Li E-mail: chuanchangli@126.com, chuanchangli@csust.edu.cn

the field of TES. Kaolinite, montmorillonite, and vermiculite, which are also layered silicate minerals, have been extensively studied in the field of TES. Li *et al.* [41] used kaolinite with different particle sizes to coat stearic acid (SA) to synthesize SA/kaolinite composite PCMs and confirmed by X-ray diffraction (XRD), Fourier transform infrared (FTIR), and other tests that no chemical reaction occurred between SA and kaolinite during the preparation process and that the SA/kaolinite composite PCMs had great chemical stability. After 200 thermal storage/release cycles, the thermal properties of the SA/kaolinite composite PCMs remained stable. Hence, SA/kaolinite composite PCMs are ideal thermal regulation materials with great application potential. Yi *et al.* [42] exfoliated natural montmorillonite (Mt) into two-dimensional montmorillonite nanosheets (MtNS), self-assembled them into a three-dimensional network montmorillonite framework (3D-MtNS), encapsulated them with SA, and prepared a high-performance composite PCM for TES. This new 3D-MtNS skeleton material has extremely high porosity, large specific surface area, and latent heat capacity of up to 198.78 $J \cdot g^{-1}$, and it can coat more than 95wt% SA without leakage, thereby showing great potential in the field of renewable energy. Xie *et al.* [43] prepared a novel shape-stabilized PCM by impregnating eutectic salt hydrate ($Na_2SO_4 \cdot 10H_2O$–$Na_2CO_3 \cdot 10H_2O$) in expanded vermiculite. The thermal conductivity of the composite PCMs was 0.192 $W \cdot m^{-1} \cdot K^{-1}$, the phase transformation temperature was 23.98°C, and the enthalpy of melting was 110.3 $J \cdot g^{-1}$. These composite PCMs have several advantages, including large heat storage capacity, suitable phase transformation temperature, and great potential in reducing building energy consumption. Given the advantages of mica minerals with unmatched structure and morphology of synthetic compounds, rich material sources, and low cost, the physical and chemical properties of mica, its thermal storage characteristics, and its combination with PCMs are worth investigating [44]. In the current work, mica and PCMs are combined to prepare high-performance composite thermal storage materials. Through this work, mica is introduced to the field of thermal storage materials, and its application potential in such materials is maximized. Mica-based composite phase change thermal storage materials can then be produced.

Polyethylene glycol (PEG) was selected as the PCM in this work because of its stable chemical properties, nontoxicity, large latent heat capacity, and suitable phase transition temperature. A novel form-stabilized composite PCM was prepared by vacuum impregnation method with PEG and mica with different meshes. The microstructure, chemical stability, and TES of the composite PCMs were investigated using XRD, FTIR, differential scanning calorimetry (DSC), thermogravimetry (TG), and thermal infrared images to explore the characteristics of mica. The form-stabilized property of the composite PCMs was tested by performing a leakage test. Relative to other supporting materials, such as expanded graphite, expanded vermiculite, and graphene, mica can be used in the field of TES without special processing. Hence, its application can reduce the production cost from the source and help promote the large-scale commercial use of PCMs for TES. At present, few reports have identified mica as a supporting matrix in the field of TES. Given the natural morphology and structure of mica minerals, as well as their wide source and low price, the application potential of mica in the field of TES is worth considering to maximize its unique advantages. By introducing mica to the field of TES, this work explores the application potential of mica as thermal storage material, broadens its application fields, and provides novel low-cost and high-performance composite PCMs for building energy conservation.

2. Experimental

2.1. Materials

Mica (100, 200, 400, 600, and 1000 mesh (100 mesh = 0.15 mm) were labeled as M_{100}, M_{200}, M_{400}, M_{600}, and M_{1000}, respectively) was obtained from Hebei Yanxi Mineral Processing Plant. The pore structure characteristics of mica with different meshes are shown in Fig. 1. PEG with an average molecular weight of 1000 (PEG) was purchased from Shanghai Zhanyun Chemical Co., Ltd.

2.2. Preparation

Mica/PEG composite PCMs were prepared by vacuum impregnation. At first, 8.0 g of PEG was added to a conical flask and heated to a melting state in a thermostatic water bath at 95°C. Exactly 4.0 g of mica with different meshes was then added. The conical flask was connected to a vacuum pump with an anti-backflow device for vacuuming to −0.1 MPa for 5 min. Thereafter, the conical flask was placed in a constant temperature water bath at 95°C and heated for 30 min. An ultrasonic water bath device was also used to further promote absorption. The composite material was filtered in a drying oven with a constant temperature of 80°C for 48 h to remove PEG that was not confined in the lamellar structure of mica. After cooling and grinding, the final samples were obtained. The composite PCMs prepared from the mica matrix of different meshes were labeled as M_{100}/PEG, M_{200}/PEG, M_{400}/PEG, M_{600}/PEG, and M_{1000}/PEG.

2.3. Characterization

The XRD patterns of the samples were obtained using D8 ADVANCE analyzer under Cu K_α radiation of 40 mA and 40 kV, scanning range of 5°–80°, and step size of 0.02°. The chemical structure of the samples was detected using FTIR (IRtracer-100AH) under the range of 400–4000 cm^{-1}. All samples were mixed with KBr to make tablets and were then measured at room temperature. The morphologies and surface structure of the samples were observed using scanning electron microscopy (SEM, Zeiss Sigma 500). DSC (Q2000) with a temperature accuracy of ±0.01°C and enthalpy precision of ±0.05% was used to obtain the phase change temperature and phase change enthalpy properties of all samples: the phase change temperature was determined by taking the

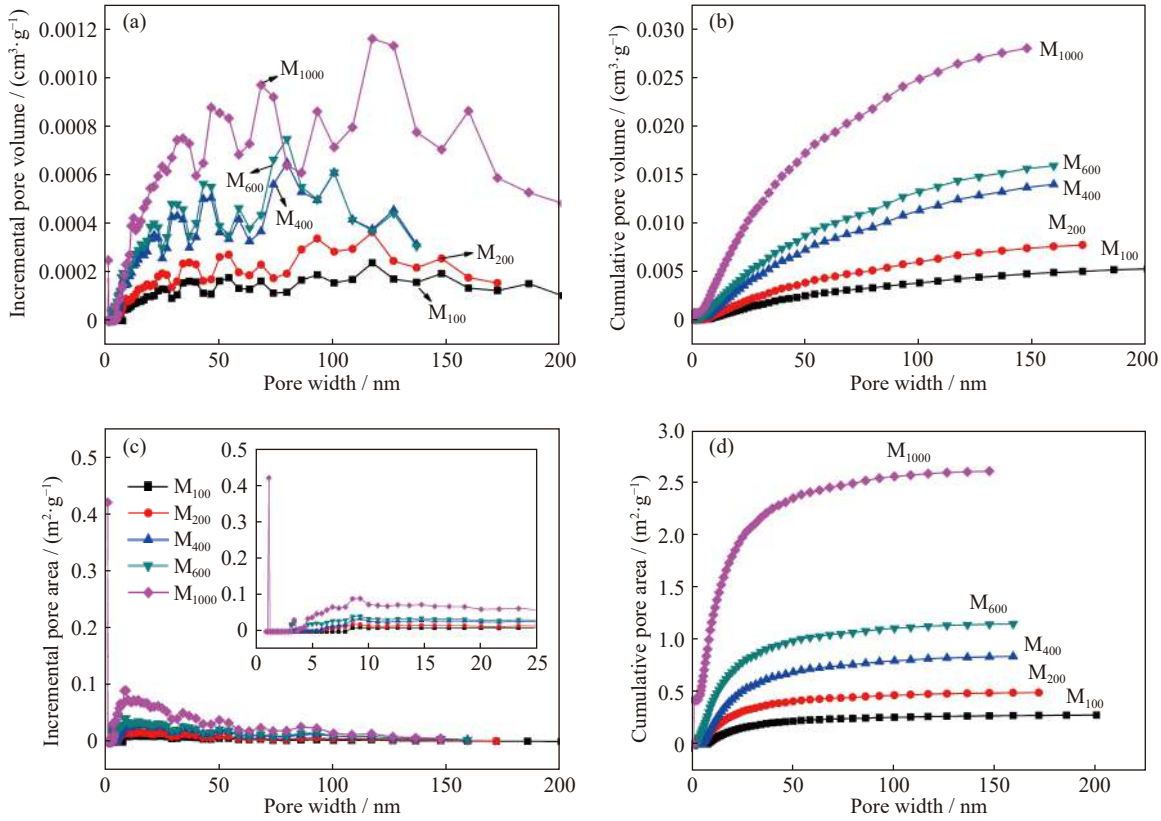

Fig. 1. Pore structure characteristics for (a) incremental pore volume, (b) cumulative pore volume, (c) incremental pore area, and (d) cumulative pore area of mica with different mesh numbers.

gradient at the point of the maximum slope on the leading edge of the peak and then extrapolating it to the baseline on that side of the peak; phase change enthalpy was calculated by numerical integration as the total area under the solid–liquid transition peak of the samples. The loading capacity of the mica-based composites was measured using a TG analyzer (HENVEN HCT-3). All samples were pressed into cylindrical disks with a size of ϕ30 mm × 2 mm under a pressure of 8 MPa. Thereafter, the DZDR-S thermal conductivity instrument for the transient planar heat source method was used to repeatedly test the thermal conductivity of the PEG and mica-based composite PCM at room temperature of 20°C; the average value of the results was then taken. The thermal infrared camera of FLUKE-Ti450 was used to record the transient temperature response behavior of pure PEG and composite PCMs during the thermal storage and release process. The leakage of the samples during the heating process was recorded by an optical camera to obtain the form-stabilized performance of the composite PCMs.

3. Results and discussion

3.1. Structure and morphology

The XRD patterns of PEG, M_{400}, and M_{400}/PEG composite PCMs are shown in Fig. 2(a). The diffraction peaks at 2θ = 8.9°, 17.8°, 26.8°, and 45.4° were attributed to mica crystal [45]. After compounding mica with PEG, the characteristic peak of mica remained in the composite material, thus proving that the crystal structure of mica was not destroyed during vacuum impregnation. Moreover, the position of the PEG peaks in the mica-based composite PCM showed no significant change and no new diffraction peak in the composite PCM curve. This result confirmed that only a physical interaction rather than a chemical reaction occurred between PEG and mica and that no new substances were formed [46]. Furthermore, this finding confirmed that the physical interaction between PEG and mica prevented leakage from the mica pores during the phase transition of PEG.

Fig. 2(b) shows the FTIR spectra of PEG, M_{400}, and M_{400}/PEG composite PCMs. In the spectra of M_{400}, the characteristic absorption peaks at 3454 and 1643 cm^{-1} were caused by the stretching and bending vibration of the −OH groups on the surface of mica, and the peaks at 1022 and 470 cm^{-1} were ascribed to the stretching vibration of Si–O and Al–O groups [47], respectively. In the spectra of PEG, the peaks at 2876 and 1470 cm^{-1} were caused by the symmetric vibration and stretching vibration of $-CH_2$ groups, respectively. The peaks at 1358 and 1280 cm^{-1} corresponded to the stretching vibration of C–O groups, and that at 1110 cm^{-1} was the result of the symmetric stretching vibration of C–O–C groups [48]. The characteristic peaks of the functional groups of mica and PEG were also reflected in the FTIR spectra of M_{400}/PEG composite PCMs, and no new characteristic peaks were generated. The results of FTIR further confirmed the physical interaction between PEG and mica and were consistent with the XRD outcomes.

Fig. 2(c) and (d) show the SEM images of M_{400} and M_{400}/PEG. The lamellar structure of mica is presented in Fig. 2(c). The lamellar structure of mica provided a good loading capacity for PEG. As shown in Fig. 2(d), the lamellar struc-

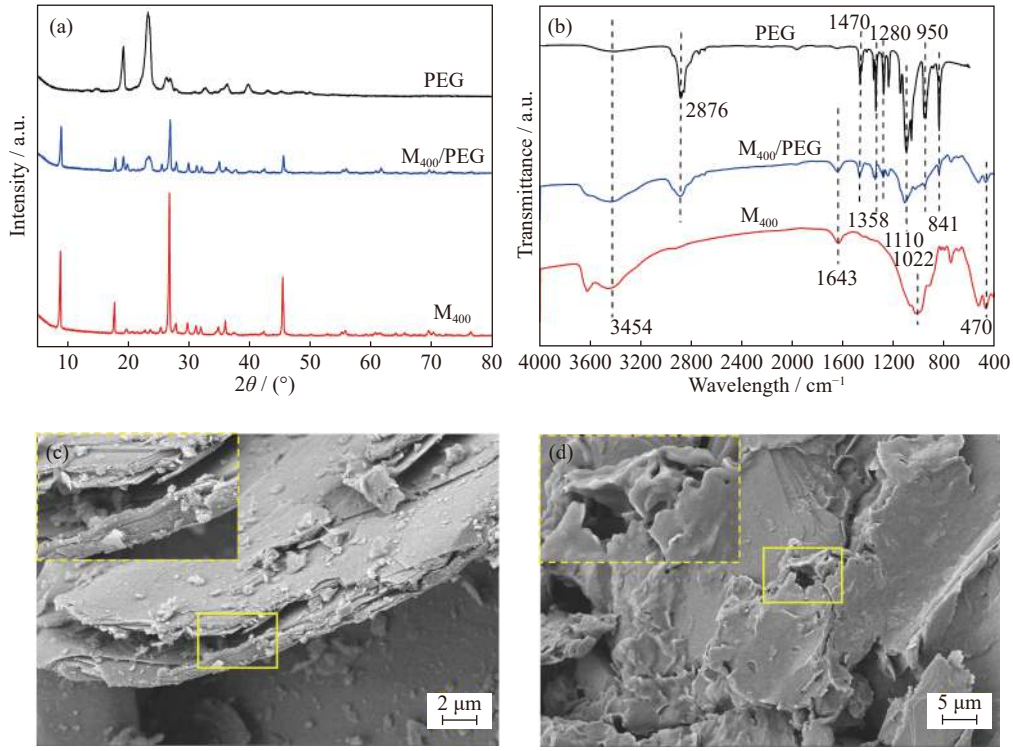

Fig. 2. XRD pattern (a) and FTIR spectra (b) of PEG, M_{400}, and M_{400}/PEG composites and SEM images of (c) M_{400} and (d) M_{400}/PEG.

ture of mica was filled with PEG, and the surface presented a smooth morphology, which confirmed that PEG was adsorbed on the surface of mica.

3.2. Thermal stability and loading capacity

The TG–DSC curves of mica and mica-based composite PCMs with different meshes are shown in Fig. 3. Fig. 3(a) presents the curve of the TG results of PEG and the prepared mica-based composites heated under nitrogen atmosphere. All samples barely showed mass loss at 180°C, thus indicating that they had great thermal stability under this temperature. As a result of the decomposition of PEG molecules, the TG curve showed a considerable decrease in the range of 350–430°C. PEG completed thermal decomposition at 500°C, and the mass loss of PEG was 91.98%. In addition, the mica-based composite PCMs had an earlier mass loss than pure PEG, possibly because the intermolecular force of pure PEG is stronger than the physical interaction between PEG and mica. As shown in Fig. 3(b), an endothermic peak formed at 400°C, corresponding to the decomposition process of the PEG molecule. The endothermic peaks of M_{100}/PEG, M_{200}/PEG, M_{400}/PEG, M_{600}/PEG, and M_{1000}/PEG were at 396, 401, 411, 409, and 410°C, respectively. Mica maintained great stability at 800°C, and the mass loss of the mica-based composite PCMs was caused by the loading of PEG. The mass loss results of M_{100}/PEG, M_{200}/PEG, M_{400}/PEG, M_{600}/PEG, and M_{1000}/PEG were obtained by TG and were equal to 42.59%, 43.78%, 46.24%, 41.58%, and 42.95%, respectively. The loading capacity of PEG (L_C, %) in the mica-based composites was calculated as

$$L_C = \frac{m_{PEG}}{m_{support}} \times 100\% = \frac{m_{PEG}}{1 - m_{PEG}} \times 100\% \quad (1)$$

where m_{PEG} and $m_{support}$ are the total mass losses of PEG (g) and mica (g), respectively. The loading capacity values of

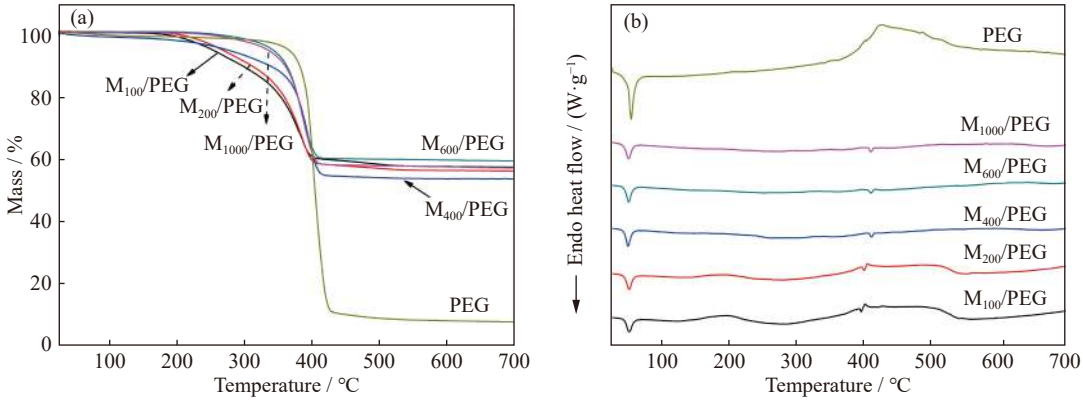

Fig. 3. TG (a) and TG–DSC (b) curves of pure PEG and mica-based composites.

PEG (L_C, %) were calculated to be 74.19%, 77.87%, 86.01%, 71.17%, and 75.28%.

3.3. Energy storage property

DSC was used to measure the phase change enthalpy of PEG and mica-based composite PCMs. Fig. 4(a) and Table 1 show the DSC results. As shown in Fig. 4(a), pure PEG had only one crystallization peak, whereas PEG in the mica matrix exhibited multiple crystallization peaks. This phenomenon indicated that the thermal storage behavior of PEG was affected after its impregnation into the mica matrix. PEG molecules were absorbed in the mica lamella structure, and the interaction between PEG and the mica matrix (including surface tension and capillary force) interfered with the crystallization process of PEG. Hence, the PEG molecules in the mica lamellar structure were not crystalized synchronously, resulting in multiple peaks during crystallization in the DSC curve. The melting phase change temperatures of PEG, M_{100}/PEG, M_{200}/PEG, M_{400}/PEG, M_{600}/PEG, and M_{1000}/PEG were 45.65, 46.02, 45.80, 46.03, 45.77, and 45.72°C, respectively. Moreover, the latent heat of melting (ΔH_m) and the latent heat of freezing (ΔH_f) were ascertained to be 170.7 J·g^{-1} and 170.7 J·g^{-1}, respectively. Table 1 shows the thermal properties of all samples. The phase change enthalpy values of M_{400}/PEG, including 77.75 J·g^{-1} for melting and 77.73 J·g^{-1} for freezing enthalpy, were higher than those of the other samples (except pure PEG). The effective energy storage per unit mass (E_{ef}) was used to evaluate the crystallization ratio (F_c) and effectiveness of PEG in different composite PCMs as follows [49]:

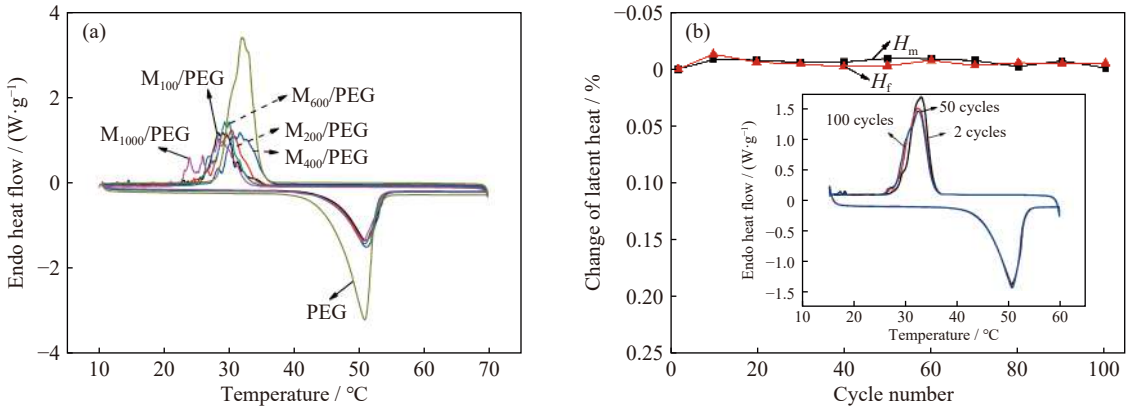

Fig. 4. (a) DSC curves of PEG and mica-based composite PCMs; (b) change of latent heat of M_{400}/PEG after 100 thermal cycles.

Table 1. Thermal properties of PEG and mica-based composites

Samples	Melting/freezing temperature, (T_m/T_f) / °C	ΔH_m / (J·g^{-1})	ΔH_f / (J·g^{-1})	Load age, β / %	L_C / %	Theoretic values of ΔH_m, ΔH_{th} / (J·g^{-1})	Crystallinity of PEG, F_c / %	Efficient energy per unit mass of PEG, E_{ef} / (J·g^{-1})
PEG	45.65/34.37	170.7	170.7	100	—	—	100	—
M_{100}/PEG	46.02/31.06	72.11	71.67	42.59	74.19	72.70	99.19	169.32
M_{200}/PEG	45.80/32.87	72.69	71.82	43.78	77.87	74.73	97.27	166.04
M_{400}/PEG	46.03/31.61	77.75	77.73	46.24	86.01	78.93	98.51	168.16
M_{600}/PEG	45.77/31.37	70.94	70.93	41.58	68.29	70.98	99.94	170.60
M_{1000}/PEG	45.72/27.52	72.27	72.05	42.95	75.28	73.32	98.57	168.26

Note: $\Delta H_{th} = \Delta H_{pure} \times \beta$.

$$F_c = \frac{\Delta H_{composite}}{\Delta H_{PCM} \times \beta} \times 100\% \quad (2)$$

$$E_{ef} = \Delta H_{PCM} \times F_c \quad (3)$$

where $\Delta H_{composite}$ and ΔH_{PCM} are the latent heat values of the composite PCMs and pure PCM, respectively; β denotes the mass fraction of the PCM in composites. As shown in Table 1, PEG in the mica-based composites exhibited excellent energy storage per unit mass (E_{ef}), M_{100}/PEG (169.32 J·g^{-1}), M_{200}/PEG (166.04 J·g^{-1}), M_{400}/PEG (168.16 J·g^{-1}), M_{600}/PEG (170.60 J·g^{-1}), and M_{1000}/PEG (168.26 J·g^{-1}); these values were close to that of pure PEG (170.7 J·g^{-1}).

The stability of M_{400}/PEG was also tested by 100 thermal cycles. As shown in Fig. 4(b), after 100 cycles of storage and release, the latent heat value changes were 0.01% and 0.048%, respectively, indicating that the prepared M_{400}/PEG possessed great stability in TES.

3.4. Thermal conductivity

As one of the important thermophysical parameters of composite PCMs, thermal conductivity reflects the ability of thermal transfer. The samples herein were subjected to multiple thermal conductivity experiments at room temperature of 20°C, and the average value was finally taken. The thermal conductivity value of pure PEG was only 0.25 W·m^{-1}·K^{-1}, which limits its practical application. The thermal conductivities of M_{100}/PEG, M_{200}/PEG, M_{400}/PEG, M_{600}/PEG, and M_{1000}/PEG were 0.53, 0.37, 0.59, 0.36, and 0.32 W·m^{-1}·K^{-1}, respectively (Fig. 5(a)). Relative to pure PEG, M_{400}/PEG showed a considerable increase in thermal conductivity of

136%.

Fig. 5(b) shows the heating and cooling temperature curves of PEG and mica-based composite PCMs. All samples were first placed in a constant thermal water bath at 65°C for simultaneous heating and then cooled at a room temperature of 18°C. A paperless recorder was used to record the temperature changes during the heating and cooling of the samples. As shown in Fig. 5(b), M_{400}/PEG had a relatively high heating rate. The temperatures of M_{400}/PEG and pure PEG after heating for 210 s were 64 and 44°C, respectively. Moreover, pure PEG and M_{400}/PEG required a cooling time of 483 s (from 44 to 41.2°C and from 64 to 38.5°C, respectively). Relative to pure PEG, the M_{400}/PEG composite showed a significantly improved thermal conductivity, indicating that M_{400}/PEG composite can quickly store and release thermal energy.

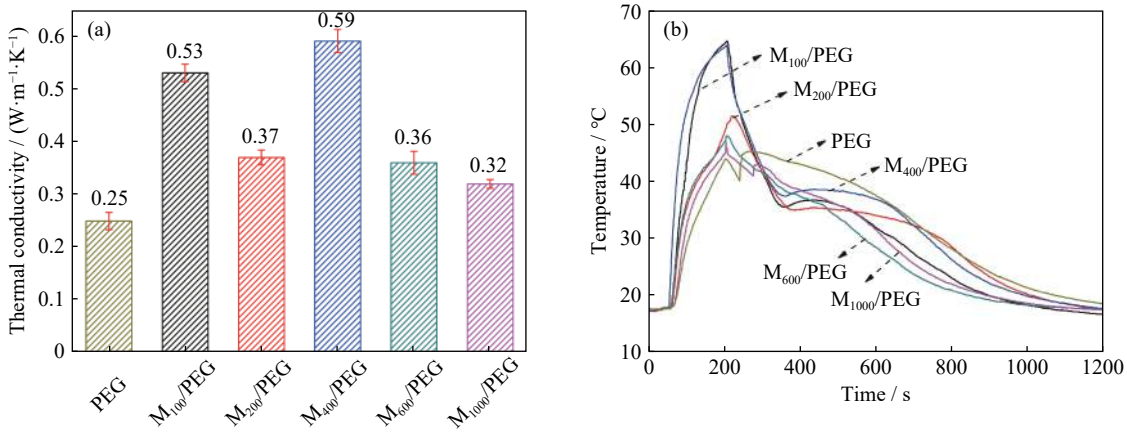

Fig. 5. (a) Thermal conductivity of PEG and mica-based composites; (b) heating and cooling temperature curves of PEG and mica-based composites.

3.5. Thermal response behavior

To show the thermal response property of the samples intuitively, this study utilized different colors in reflecting the temperatures of the samples at different times that were obtained using a thermal infrared camera. First, all samples were compressed into plates of the same size (ϕ20 mm × 2 mm) under the same pressure and then put into a mold made of foil to ensure their even heating and avoid leakage during the heating process. A thermostatic heating plate (DB-XAB) was used to maintain a constant temperature of 70±1°C.

Fig. 6(a) and (b) show the infrared images of PEG and M_{400}/PEG, in which different colors represent different temperatures. Relative to pure PEG, M_{400}/PEG was heated quickly from room temperature (20°C) to 44.1°C after 55 s. At this time, the temperature of PEG was only 39.6°C (Fig. 6(a)). This trend was consistent with that shown in Fig. 6(c). During the cooling process, the temperature of M_{400}/PEG dropped from 60 to 34.1°C after 22 s, while that of PEG remained high at 47.1°C (Fig. 6(b)). At 178 s, the temperature of M_{400}/PEG reduced to room temperature, while that of PEG remained at high (Fig. 6(c)). This result indicated that M_{400}/PEG composite PCMs can respond more quickly to temperature changes than pure PEG during the thermal storage and release process.

3.6. Form-stabilized property

Maintaining the stability of the shape structure is essential for form-stabilized composite PCMs. The changes of the samples during the heating process were recorded using an optical camera. At first, the same masses of PEG and M_{400}/PEG were weighed. Then, the two samples were pressed into a cylindrical shape of (ϕ20 mm × 2 mm) under a pressure of 8 MPa. The pressed samples were placed on the

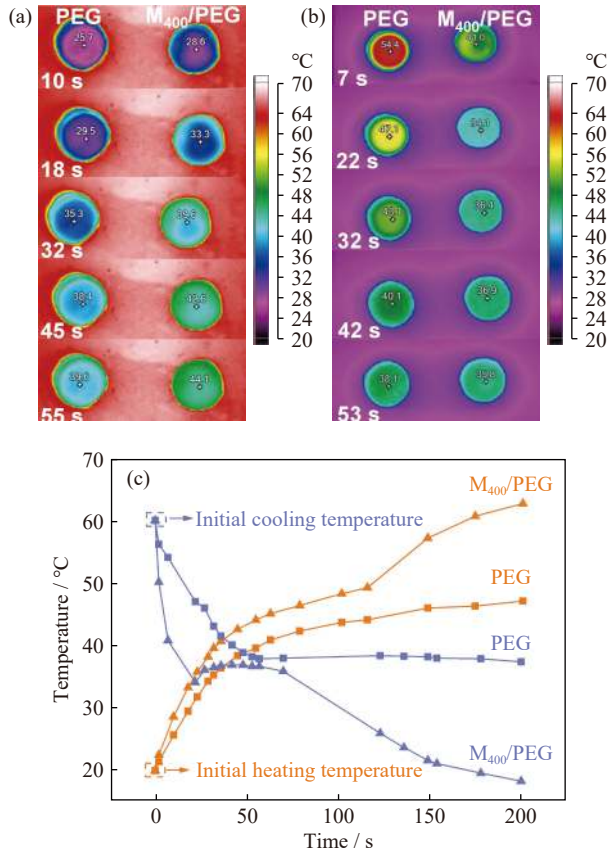

Fig. 6. Thermal infrared images of PEG and M_{400}/PEG during (a) heating and (b) cooling; (c) temperature response curves of PEG and M_{400}/PEG during heating and cooling.

thermostatic heating plate under 80°C. A graphene plate was placed on the heating plate to ensure the even heating of the samples. The leakage areas of PEG and M_{400}/PEG in the heating process were compared and were regarded as the diameter of melted PCM.

As shown in Fig. 7(a), PEG melted at 90 s and completely melted into liquid form after 300 s, while M_{400}/PEG maintained its initial shape during the whole heating process. This experimental result confirmed that the lamellar structure of mica can effectively limit leakage during the solid–liquid phase transformation process of PEG.

The melting behavior of PEG is described by leakage diameter ($D_{leakage}$), initial sample diameter (D_{sample}), and instantaneous sample diameter (D'_{sample}). $D_{leakage}/D_{sample}$ is used to represent the leakage status in the PEG heating process, and D'_{sample}/D_{sample} is used to represent the melting status. As shown in Fig. 7(b), with the increase of heating time, the leakage area gradually increased because of the solid–liquid phase transformation of PEG. Meanwhile, the instantaneous diameter of PEG gradually decreased because of melting. After 300 s, the D'_{sample}/D_{sample} percentage was zero, indicating the complete melting of solid PEG. The form-stabilized test showed that mica, as a supporting matrix, can effectively restrict molten PEG in the lamellar structure, maintain a stable shape structure, and provide the M_{400}/PEG composite with excellent form-stabilized property.

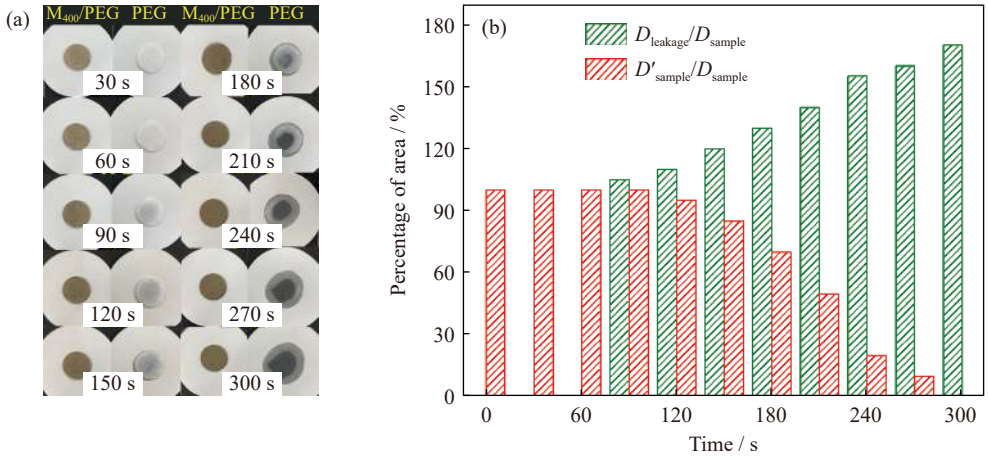

Fig. 7. (a) Optical photographs of PEG and M_{400}/PEG composite heated at 80°C for different times; (b) diameter ratio of leakage area of cylindrical compressed PEG.

4. Conclusion

In this work, mica-based composites (M_{100}/PEG, M_{200}/PEG, M_{400}/PEG, M_{600}/PEG, and M_{1000}/PEG) were prepared by absorbing PEG into mica-based support through the vacuum impregnation method. M_{100}/PEG, M_{200}/PEG, M_{400}/PEG, M_{600}/PEG, and M_{1000}/PEG composites melted at 46.02, 45.80, 46.03, 45.77, and 45.72°C, respectively. The values of the latent heat of melting of M_{100}/PEG, M_{200}/PEG, M_{400}/PEG, M_{600}/PEG, and M_{1000}/PEG were 72.11, 72.69, 77.75, 70.94, and 72.27 $J \cdot g^{-1}$, respectively. The thermal conductivity of the M_{400}/PEG composite greatly increased by 136% relative to that of pure PEG (0.25 $W \cdot m^{-1} \cdot K^{-1}$). The thermal infrared images showed that the M_{400}/PEG composite responded quickly to the change of external temperature. The leakage experiment results showed that the mica matrix prevented PEG phase change leakage and that the composite PCMs had great form-stabilized properties. In conclusion, the unique morphology and lamellar structure of mica make it capable of preventing the leakage of PCMs. M_{400}/PEG composite has superior thermal storage performance and can be used in the field of building energy conservation. Through its combination with building materials, intelligent building materials with thermal energy and release functions can be developed to reduce indoor temperature fluctuations and create a comfortable indoor environment.

Acknowledgements

This work was financially supported by the National Natural Science Foundation of China (Nos. 51874047 and 51504041), the Special Fund for the Construction of Innovative Provinces in Hunan Province, China (No. 2020RC3038), the Changsha City Fund for Distinguished and Innovative Young Scholars, China (No. kq1802007), the Fund for University Young Core Instructors of Hunan Province, China, the Innovation Program for Postgraduate of Changsha University of Science and Technology, China, and the Outstanding Youth Project of Hunan Provincial Department of Education, China (No. 18B148).

Conflict of Interest

The authors declare no potential conflict of interest.

References

[1] A. Sarı, A. Bicer, A. Al-Ahmed, F.A. Al-Sulaiman, M.H. Zahir, and S.A. Mohamed, Silica fume/capric acid-palmitic acid composite phase change material doped with CNTs for thermal energy storage, *Sol. Energy Mater. Sol. Cells*, 179(2018), p. 353.

[2] P.M. Hou, M.H. Qin, S.Q. Cui, and K. Zu, Preparation and characterization of metal-organic framework /microencapsulated phase change material composites for indoor hygrotherm-

al control, *J. Build. Eng.*, 31(2020), art. No. 101345.
[3] F.Q. Zhou, F. Qin, Z. Yi, W.T. Yao, Z.M. Liu, X.W. Wu, and P.H. Wu, Ultra-wideband and wide-angle perfect solar energy absorber based on Ti nanorings surface plasmon resonance, *Phys. Chem. Chem. Phys.*, 23(2021), No. 31, p. 17041.
[4] Y.Q. Jiang, G. Cheng, Y.H. Li, Z.X. He, J. Zhu, W. Meng, L. Dai, and L. Wang, Promoting vanadium redox flow battery performance by ultra-uniform ZrO_2@C from metal-organic framework, *Chem. Eng. J.*, 415(2021), art. No. 129014.
[5] R.D. Beltrán and J. Martínez-Gómez, Analysis of phase change materials (PCM) for building wallboards based on the effect of environment, *J. Build. Eng.*, 24(2019), art. No. 100726.
[6] Y.N. Gao, F. He, X. Meng, Z.Y. Wang, M. Zhang, H.T. Yu, and W.J. Gao, Thermal behavior analysis of hollow bricks filled with phase-change material (PCM), *J. Build. Eng.*, 31(2020), art. No. 101447.
[7] B.J. Nie, Z. Du, B.Y. Zou, Y.L. Li, and Y.L. Ding, Performance enhancement of a phase-change-material based thermal energy storage device for air-conditioning applications, *Energy Build.*, 214(2020), art. No. 109895.
[8] Y.L. Zhu, Y. Chi, S.E. Liang, X. Luo, K.P. Chen, C.R. Tian, J.H. Wang, and L. Zhang, Novel metal coated nanoencapsulated phase change materials with high thermal conductivity for thermal energy storage, *Sol. Energy Mater. Sol. Cells*, 176(2018), p. 212.
[9] T.T. Wang, C.P. Li, X.S. Xie, B.A. Lu, Z.X. He, S.Q. Liang, and J. Zhou, Anode materials for aqueous zinc ion batteries: Mechanisms, properties, and perspectives, *ACS Nano*, 14(2020), No. 12, p. 16321.
[10] X. Min, J. Xiao, M.H. Fang, W.A. Wang, Y.J. Zhao, Y.G. Liu, A.M. Abdelkader, K. Xi, R.V. Kumar, and Z.H. Huang, Potassium-ion batteries: Outlook on present and future technologies, *Energy Environ. Sci.*, 14(2021), No. 4, p. 2186.
[11] T. Qiu, J.G. Yang, and X.J. Bai, Insight into the change in carbon structure and thermodynamics during anthracite transformation into graphite, *Int. J. Miner. Metall. Mater.*, 27(2020), No. 2, p. 162.
[12] B. Yilmaz, B. Yüksel, G. Orhan, D. Aydin, and Z. Utlu, Synthesis and characterization of salt-impregnated anodic aluminum oxide composites for low-grade heat storage, *Int. J. Miner. Metall. Mater.*, 27(2020), No. 1, p. 112.
[13] Y.X. Yu, Y.F. Zhou, Y.J. Zhang, Y.Q. Zhang, X.D. Liu, X.J. Liang, J.P. Liu, S.Q. Chen, and W.D. Xiang, Novel $CsPbX_3$@mica composites with excellent optical properties for high efficiency and wide color gamut white light-emitting diode, *J. Lumin.*, 236(2021), art. No. 118129.
[14] V. Kashyap, S. Sakunkaewkasem, P. Jafari, M. Nazari, B. Eslami, S. Nazifi, P. Irajizad, M.D. Marquez, T.R. Lee, and H. Ghasemi, Full spectrum solar thermal energy harvesting and storage by a molecular and phase-change hybrid material, *Joule*, 3(2019), No. 12, p. 3100.
[15] M.A. Gerkman and G.G.D. Han, Toward controlled thermal energy storage and release in organic phase change materials, *Joule*, 4(2020), No. 8, p. 1621.
[16] Y.L. Song, N. Zhang, Y.G. Jing, X.L. Cao, Y.P. Yuan, and F. Haghighat, Experimental and numerical investigation on dodecane/expanded graphite shape-stabilized phase change material for cold energy storage, *Energy*, 189(2019), art. No. 116175.
[17] M.C. Browne, B. Norton, and S.J. McCormack, Phase change materials for photovoltaic thermal management, *Renewable Sustainable Energy Rev.*, 47(2015), p. 762.
[18] A. Papadimitratos, S. Sobhansarbandi, V. Pozdin, A. Zakhidov, and F. Hassanipour, Evacuated tube solar collectors integrated with phase change materials, *Sol. Energy*, 129(2016), p. 10.
[19] J. Triano-Juárez, E.V. Macias-Melo, I. Hernández-Pérez, K.M. Aguilar-Castro, and J. Xamán, Thermal behavior of a phase change material in a building roof with and without reflective coating in a warm humid zone, *J. Build. Eng.*, 32(2020), art. No. 101648.
[20] M.Y. Luo, J.Q. Song, Z.Y. Ling, Z.G. Zhang, and X.M. Fang, Phase change material coat for battery thermal management with integrated rapid heating and cooling functions from −40°C to 50°C, *Mater. Today Energy*, 20(2021), art. No. 100652.
[21] Z.J. An, L. Jia, Y. Ding, C. Dang, and X.J. Li, A review on lithium-ion power battery thermal management technologies and thermal safety, *J. Therm. Sci.*, 26(2017), No. 5, p. 391.
[22] Y. Lu, X.D. Xiao, J. Fu, C.M. Huan, S. Qi, Y.J. Zhan, Y.Q. Zhu, and G. Xu, Novel smart textile with phase change materials encapsulated core-sheath structure fabricated by coaxial electrospinning, *Chem. Eng. J.*, 355(2019), p. 532.
[23] X. Min, B. Sun, S. Chen, M.H. Fang, X.W. Wu, Y.G. Liu, A. Abdelkader, Z.H. Huang, T. Liu, K. Xi, and R. Vasant Kumar, A textile-based SnO_2 ultra-flexible electrode for lithium-ion batteries, *Energy Storage Mater.*, 16(2019), p. 597.
[24] Z.D. Tang, H.Y. Gao, X. Chen, Y.F. Zhang, A. Li, and G. Wang, Advanced multifunctional composite phase change materials based on photo-responsive materials, *Nano Energy*, 80(2021), art. No. 105454.
[25] L. Yang, Y.P. Yuan, N. Zhang, Y.F. Dong, Y.F. Sun, and W.H. Ji, Photo-to-thermal conversion and energy storage of lauric acid/expanded graphite composite phase change materials, *Int. J. Energy Res.*, 44(2020), No. 11, p. 8555.
[26] C. Confalonieri, A.T. Grimaldi, and E. Gariboldi, Ball-milled Al–Sn alloy as composite Phase Change Material, *Mater. Today Energy*, 17(2020), art. No. 100456.
[27] Y.Y. Cui, Y.J. Ke, C. Liu, Z. Chen, N. Wang, L.M. Zhang, Y. Zhou, S.C. Wang, Y.F. Gao, and Y. Long, Thermochromic VO_2 for energy-efficient smart windows, *Joule*, 2(2018), No. 9, p. 1707.
[28] Y. Zhou, S.C. Wang, J.Q. Peng, Y.T. Tan, C.C. Li, F.Y.C. Boey, and Y. Long, Liquid thermo-responsive smart window derived from hydrogel, *Joule*, 4(2020), No. 11, p. 2458.
[29] X.H. Bao, Y.Y. Tian, L. Yuan, H.Z. Cui, W.C. Tang, W.H. Fung, and H. Qi, Development of high performance PCM cement composites for passive solar buildings, *Energy Build.*, 194(2019), p. 33.
[30] Y.X. Lin, Y.T. Jia, G. Alva, and G.Y. Fang, Review on thermal conductivity enhancement, thermal properties and applications of phase change materials in thermal energy storage, *Renewable Sustainable Energy Rev.*, 82(2018), p. 2730.
[31] Y.Y. Deng and L.J. Yang, Preparation and characterization of polyethylene glycol (PEG) hydrogel as shape-stabilized phase change material, *Appl. Therm. Eng.*, 114(2017), p. 1014.
[32] S.A. Memon, H.Z. Cui, H. Zhang, and F. Xing, Utilization of macro encapsulated phase change materials for the development of thermal energy storage and structural lightweight aggregate concrete, *Appl. Energy*, 139(2015), p. 43.
[33] Y.J. Zhao, X. Min, Z.H. Huang, Y.G. Liu, X.W. Wu, and M.H. Fang, Honeycomb-like structured biological porous carbon encapsulating PEG: A shape-stable phase change material with enhanced thermal conductivity for thermal energy storage, *Energy Build.*, 158(2018), p. 1049.
[34] N. Zhang and Y.P. Yuan, Synthesis and thermal properties of nanoencapsulation of paraffin as phase change material for latent heat thermal energy storage, *Energy Built Environ.*, 1(2020), No. 4, p. 410.
[35] M.M. Joybari, F. Haghighat, S. Seddegh, and Y.P. Yuan, Simultaneous charging and discharging of phase change materials: Development of correlation for liquid fraction, *Sol. Energy*, 188(2019), p. 788.
[36] C.Z. Liu, Z.H. Rao, J.T. Zhao, Y.T. Huo, and Y.M. Li, Review on nanoencapsulated phase change materials: Preparation, characterization and heat transfer enhancement, *Nano Energy*, 13(2015), p. 814.

[37] C.C. Li, X.B. Zhao, B. Zhang, B.S. Xie, Z.X. He, J. Chen, and J.J. He, Stearic acid/copper foam as composite phase change materials for thermal energy storage, *J. Therm. Sci.*, 29(2020), No. 2, p. 492.
[38] L.X. Chai, X.D. Wang, and D.Z. Wu, Development of bifunctional microencapsulated phase change materials with crystalline titanium dioxide shell for latent-heat storage and photocatalytic effectiveness, *Appl. Energy*, 138(2015), p. 661.
[39] X.B. Huang, X. Chen, A. Li, D. Atinafu, H.Y. Gao, W.J. Dong, and G. Wang, Shape-stabilized phase change materials based on porous supports for thermal energy storage applications, *Chem. Eng. J.*, 356(2019), p. 641.
[40] Y.J. Zhao, X. Min, Z.P. Ding, S. Chen, C.Z. Ai, Z.L. Liu, T.Z. Yang, X.W. Wu, Y.G. Liu, S.W. Lin, Z.H. Huang, P. Gao, H. Wu, and M.H. Fang, Metal-based nanocatalysts via a universal design on cellular structure, *Adv. Sci.*, 7(2020), No. 3, art. No. 1902051.
[41] J.W. Li, X.C. Zuo, X.G. Zhao, D.K. Li, and H.M. Yang, Stearic acid hybridizing kaolinite as shape-stabilized phase change material for thermal energy storage, *Appl. Clay Sci.*, 183(2019), art. No. 105358.
[42] H. Yi, Z. Ai, Y.L. Zhao, X. Zhang, and S.X. Song, Design of 3D-network montmorillonite nanosheet/stearic acid shape-stabilized phase change materials for solar energy storage, *Sol. Energy Mater. Sol. Cells*, 204(2020), art. No. 110233.
[43] N. Xie, J.M. Luo, Z.P. Li, Z.W. Huang, X.N. Gao, Y.T. Fang, and Z.G. Zhang, Salt hydrate/expanded vermiculite composite as a form-stable phase change material for building energy storage, *Sol. Energy Mater. Sol. Cells*, 189(2019), p. 33.
[44] C.M. Jia, X.Y. Zhao, Y.H. Lai, J.J. Zhao, P.C. Wang, D.S. Liou, P. Wang, Z.H. Liu, W.H. Zhang, W. Chen, Y.H. Chu, and J.Y. Li, Highly flexible, robust, stable and high efficiency perovskite solar cells enabled by van der Waals epitaxy on mica substrate, *Nano Energy*, 60(2019), p. 476.
[45] B. Ilić, V. Radonjanin, M. Malešev, M. Zdujić, and A. Mitrović, Effects of mechanical and thermal activation on pozzolanic activity of kaolin containing mica, *Appl. Clay Sci.*, 123(2016), p. 173.
[46] B.T. Tang, H.P. Wei, D.F. Zhao, and S.F. Zhang, Light-heat conversion and thermal conductivity enhancement of PEG/SiO_2 composite PCM by *in situ* Ti_4O_7 doping, *Sol. Energy Mater. Sol. Cells*, 161(2017), p. 183.
[47] H.B. Dai, H.X. Li, and F.H. Wang, An alternative process for the preparation of Cu-coated mica composite powder, *Surf. Coat. Technol.*, 201(2006), No. 6, p. 2859.
[48] A. Reddy Polu and R. Kumar, Impedance spectroscopy and FTIR studies of PEG-based polymer electrolytes, *J. Chem.*, 8(2011), No. 1, p. 347.
[49] C.C. Li, B.S. Xie, D.L. Chen, J. Chen, W. Li, Z.S. Chen, S.W. Gibb, and Y. Long, Ultrathin graphite sheets stabilized stearic acid as a composite phase change material for thermal energy storage, *Energy*, 166(2019), p. 246.